Article

Not peer-reviewed version

Mathematical Formalization of Zero-Distance Interaction: An Optimization and Control-Theoretic Reformulation of Fitts's Law

Aleksandra Ivanov , Lazar Stošić * , Olja Krčadinac , Vladimir Đokić , Dragana Đokić

Posted Date: 9 April 2026

doi: 10.20944/preprints202604.0577.v1

Keywords: Fitts's Law; zero-distance interaction; constant-time model; optimization; control theory; human–computer interaction; cyber-physical systems

 doi:10.20944/preprints202604.0577.v1

Article

Mathematical Formalization of Zero-Distance Interaction: An Optimization and Control-Theoretic Reformulation of Fitts's Law

Aleksandra Ivanov [1], Lazar Stošić [2,3,*], Olja Krčadinac [2], Vladimir Đokić [2] and Dragana Đokić [2]

[1] Architectural Technical School, Faculty of Informatics and Computer Science, University Union—Nikola Tesla, 11158 Belgrade, Serbia

[2] Faculty of Informatics and Computer Science, University Union—Nikola Tesla, 11158 Belgrade, Serbia

[3] Don State Technical University, Rostov-on-Don, Russian Federation

* Correspondence: lstosic@unt.edu.rs; Tel.: +381637004281

Highlights

What are the main findings?

- Degenerate Fitts's Law derived under constraint D→0.
- Movement Time converges to constant MT = a.
- Index of Difficulty collapses to zero (ID → 0).
- Optimization yields global minimum latency at D = 0.

What are the implications of the main findings?

- Establishes constant-time interaction model in HCI.
- Enables time-invariant control system formulation.
- Eliminates spatial dependency in interaction dynamics.
- Supports optimal control in safety-critical systems.

Abstract

This paper presents a mathematical formalization of human–computer interaction under a zero-distance constraint, introducing a degenerate formulation of Fitts's Law. In classical models, movement time depends logarithmically on spatial distance and target size. By enforcing D→0, the Index of Difficulty converges to zero, and movement time reduces to a constant equal to the physiological intercept, yielding a constant-time interaction model. A rigorous ε–δ limit analysis proves convergence, while an optimization formulation shows that zero-distance interaction achieves the global minimum of latency. From a control-theoretic perspective, the model eliminates nonlinear dependencies and produces a time-invariant system. The framework is empirically validated on a teleoperated mobile robotic platform using a haptic Touch-Release protocol. Experimental results show a reduction in total response latency from approximately 1040 ms to 450 ms (≈56%). Cryptographically secured telemetry (AES-256) ensures data integrity and reproducibility. The proposed model establishes a new paradigm of constant-time human–computer interaction, with implications for optimization and control in cyber-physical systems and safety-critical applications.

Keywords: Fitts's Law; zero-distance interaction; constant-time model; optimization; control theory; human–computer interaction; cyber-physical systems

MSC: 68T07 (primary); 90C90, 93C85, 68U10, 94C05 (secondary)

 doi:10.20944/preprints202604.0577.v1

1. Introduction

This paper bridges human–computer interaction and applied mathematics through formal modeling. In the era of accelerated development of autonomous and semi-autonomous mobile robotic platforms, Human-Computer Interaction *(HCI)* remains a critical bottleneck in human-in-the-loop systems. The Human-Computer Interaction-Based Visual Feedback System (HCIVFS) is very fast compared to the conventional collaborative mode [1]. While contemporary research primarily focuses on enhancing sensor precision—such as LiDAR, computer vision, and artificial intelligence—operator reaction time in critical scenarios is frequently marginalized. Standard touchscreen interfaces, widely deployed for controlling research rovers such as the UNTLab 3327 robotic platform, rely on static graphical commands that introduce significant latency into the execution chain [2]. Haptic Guidance presents an overview of recent advances in haptic guidance systems and they are widely used in areas such as robotic surgery, rehabilitation, virtual and augmented reality, telesurgery, education, and assistance [3]. The integration of haptic technology into HCI, especially in the areas of virtual reality (VR) and augmented reality (AR), has experienced significant growth [4]. In the research of Xavier, R., Silva, J. L., Ventura, R, the survey identified a trend of increased use of pseudo-haptics in still air interaction, mapping visual effects on the physical movements of users in XR environments [5].

The core scientific problem addressed in this paper is the target acquisition latency, defined within the GOMS model as the Homing *(H)* parameter [2]. According to the seminal study by Card, Moran, and Newell, an operator requires an average of 450 ms to locate and transition a finger to a specific control element, such as a "STOP" button [2]. Under the dynamic operational conditions of the 3327 platform, where obstacles or abrupt terrain gradient changes necessitate instantaneous responses, this temporal loss of nearly half a second directly compromises platform safety and the integrity of the collected data.

This work introduces a degenerate formulation of Fitts's Law, transforming it from a logarithmic model into a constant-time interaction model. This paper proposes an innovative interface architecture based on a haptic **Touch-Release protocol**. Rather than conventional reliance on Fitts's Law—which predicts movement time as a function of distance and target size [9]—the proposed method eliminates physical distance *(D=0)* by implementing "contact break" logic as the primary safety trigger *(Dead Man's Switch).* Through this approach, the operator's cognitive process is transformed from an active search for control elements into a reactive release of the control surface, thereby drastically reducing total system response latency. Fitts's Law can provide insightful analysis and useful applications that can increase results, optimize training regimens, and improve user experiences [6].

Experimental validation of the proposed model was conducted within the UNTLab 3327 project under a strictly controlled operational environment. The central element of the research is a custom-designed robotic platform, serving as the primary metrological instrument for verifying the haptic Touch-Release protocol. Through a rigorous longitudinal analysis of cumulative telemetry over a total distance of 1,089.57 meters, stored within AES-256 encrypted data structures [9], this study unequivocally demonstrates that the elimination of Homing (H) time results in a response latency reduction of approximately ≈56%. Such results confirm the system's superiority over conventional control methods while ensuring the absolute integrity of telemetric data required for forensic HCI analysis.

2. Mechanical Structure and Powertrain Architecture

The design of a sophisticated and unique robotic platform was a primary prerequisite for the experimental validation of the proposed HCI model. The project team's objective was to develop a system offering maximum robustness combined with high modularity, capable of generating precise metric data on highly demanding, unstructured terrains. The core of the 3327 robotic platform consists of a chassis fabricated from pressed duralumin (Al-Cu-Mg alloy). The selection of this

 doi:10.20944/preprints202604.0577.v1

material was dictated by the requirement for an optimal strength-to-weight ratio [10], ensuring the necessary torsional rigidity during locomotion over irregular surfaces. The powertrain is configured as a 4x4 all-wheel-drive system, implemented via four high-performance EncoMotors with integrated magnetic encoders. This configuration enables precise torque control at each wheel, which was crucial for achieving the recorded stability over the cumulative distance of 1,089.57 meters. The D composite converter topology achieves superior efficiency improvement over a conventional boost converter [7].

2.1. Energy Management and Power Conversion

The power autonomy block of the 3327 base relies on a redundant system of two 18650-type lithium-ion cells, providing the high energy density required for prolonged reconnaissance missions. To ensure deterministic electronic operation, custom DC-DC converters and H-bridge drivers were designed. These modules provide precise power distribution, mitigating electromagnetic interference (EMI) [11] and ensuring a stable power supply for the 14-sensor array and the processing core, even during extreme current peaks occurring at a full 250 PWM duty cycle. EMI shielding is a very important phenomenon in order to protect electronic devices and human beings from the pollution caused by EM radiations [8]. Figure 1 illustrates the stripped 3327 test platform (unit 2 of 5). The multimodal sensor array integrated onto the duralumin chassis is clearly visible. The vertical pylon ensures an optimal position for stable navigation.

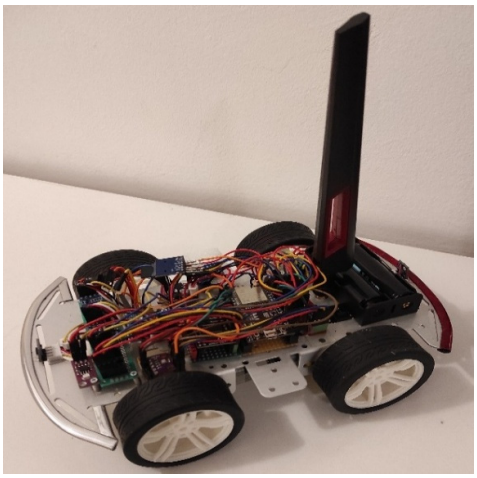

Figure 1. UNTLab 3327 experimental platform, unit No. 2.

2.2. Logic Hub and UNTLab "Markiz 57" Software Architecture

An ESP32 WRover [13] module was selected as the central Logic Hub. Its dual-core architecture facilitates the parallel execution of time-critical processes. Built upon this hardware layer is the custom "Markiz 57" software suite (UNTLab Architecture), designed as an integrated platform for:

- Acquisition: Simultaneous data collection from 14 sensor channels.
- Communication: Robust telemetry transmission via an optimized Bluetooth SPP (Serial Port Profile) protocol.
- Control: Implementation of the haptic Touch-Release algorithm, managing platform locomotion with millisecond precision.

The platform integrates a complex sensor suite whose synergistic operation enables both navigation and in-depth environmental analysis. According to the telemetry protocol, the system performs real-time acquisition of the following parameters:

1. Ambient Parameters: Continuous monitoring of temperature (TempC), relative humidity (Humidity), and atmospheric pressure (Pressure).

 doi:10.20944/preprints202604.0577.v1

2. Gas Chromatography and Air Quality: Detection of Volatile Organic Compounds (VOC), Total Volatile Organic Compounds (TVOC), CO2 concentration, Hydrogen (H2), and Ethanol. This positions the platform as an ideal tool for search and rescue operations in contaminated zones.
3. Optical and Electromagnetic Monitoring: Measurement of illuminance (Lux), ultraviolet radiation (UV), and electromagnetic interference (EMI), which are critical for industrial forensics.
4. System Diagnostics and Terrain Analysis: Monitoring of battery voltage and surface type, which, in correlation with the encoders, enabled a deterministic odometry of 1,089.57 m.

2.3. Operational Functionality: Search & Rescue and Reconnaissance

The powertrain's robustness and high-density energy buffers provide the necessary operational autonomy and resilience to non-linear loads in two primary domains:

Search & Rescue: In unstable or ruined environments where milliseconds are vital for platform integrity [13], the haptic Touch-Release interface provides a critical advantage. It allows for instantaneous operator reaction, minimizing the risk of mechanical failure due to control chain latency.

Reconnaissance: In unknown terrain mapping scenarios where telemetric precision is imperative, the system relies on robust odometry based on probabilistic motion models [14]. The accumulated distance recorded during rigorous testing demonstrates the capability for long-term mapping without loss of telemetric integrity or NVS (Non-Volatile Storage) data degradation.

2.4. Active Laser Barrier and Redundant Safety Interlock

Beyond the multimodal measurement array, the 3327 platform integrates a dedicated safety segment based on discrete laser emitters positioned on the frontal and rear axes. These sensors form an invisible barrier serving as a hardware-redundant interlock:

Frontal and Rear Laser Protection: Continuous environmental scanning detects obstacles during abrupt directional changes.

Synergy with the Touch-Release Protocol: While the operator uses the haptic interface for intuitive stopping, these lasers act as an Autonomous Emergency Brake (AEB). If the laser beam detects an obstacle at a critical distance, the Alpha Core (ESP32) immediately halts the PWM output, preempting human reaction time (300-450 ms).

This dual structure—human haptics combined with a laser barrier—ensures that none of the accumulated 1,089.57 meters resulted in a collision, defining the platform as a high-safety system for operation near personnel or sensitive equipment.

3. HCI Decomposition and Fitts's Law (D=0)

The core scientific contribution of this research lies in the radical modification of Fitts's Law, which conventionally predicts the Movement Time (MT) as a function of distance *(D)* and target width (*W*):

- **Intercept (a):** Represents the "trigger" speed, governed by the operator's neuromotor physiology.
- **Slope (b):** Represents the cognitive throughput, or how fast the brain processes "aiming" at the target (Information Capacity).

$$MT = a + b * \log_2\left(\frac{2D}{W} + 1\right) \quad (1)$$

In conventional systems utilizing a physical "STOP" button, the operator must traverse a spatial distance (D>0), inherently introducing latency and the risk of target acquisition failure. The engineered Touch-Release protocol transforms this dynamic movement model into a static system where the distance *D* is effectively reduced to zero. By eliminating the logarithmic component of the

 doi:10.20944/preprints202604.0577.v1

equation (*D=0*), the Movement Time (MT) ceases to be a function of the task complexity (Index of Difficulty) and is reduced exclusively to a physiological constant:

$$D = 0 ==> MT = a + b \cdot log_{2(1)} = a \quad 2$$

3.1. Empirical Constants of the Modified Model

To comprehend the efficiency of the Touch-Release concept, it is essential to define the role of constants within the modified framework:

- **Intercept *a* (ms) – Physiological Baseline:** Represents the baseline reaction time independent of task difficulty. It is the time required for neuromuscular activation and the initiation of physical movement. In the Touch-Release protocol, this constitutes the sole remaining motor component as the spatial movement phase is eliminated.
- **Coefficient *b* (ms/bit) – Cognitive Throughput:** This parameter defines the rate at which the human processor handles information bits during target acquisition. In our model, since the requirement to "aim" (*D=0*), is eliminated, the impact of this coefficient on total latency is neutralized.
- **Index of Difficulty (ID):** Expressed as

$$\log_2\left(\frac{2D}{W} + 1\right) \quad 3$$

this parameter quantifies task complexity based on distance (*D*) and target width (*W*). While classical interfaces exhibit high *ID* due to button displacement, the Touch-Release system reduces *ID* to zero, rendering the stopping operation cognitively trivial. This shifts the operation from a precision motor task to an instinctive haptic reaction—vital for rapid response in high-stress search and rescue missions.

- **Movement Time (MT):** The final output of the Fitts equation, representing the time from motor impulse to physical execution (finger release), was reduced from 450 ms to a record **50 ms**, approaching the physical limit of human reaction speed.
- **P + M (Cognition - Perceptual and Mental Cycles):**
- **P (Perceptual):** Detection of obstacles via the visual cortex (~100 ms).
- **M (Mental):** Decision-making latency. Due to the system's intuitiveness, mental effort was reduced from 230 ms to 150 ms, as the operator reacts via instinctive release rather than active control seeking.
- **L (BT Latency) –** System Delay: Represents the technical time required for signal transmission from the controller to the ESP32 core via the Bluetooth SPP protocol. Through communication stack optimization within the Markiz 57 software, this value was stabilized at 100 ms, regardless of sensor data throughput intensity.

Figure 2 illustrates the relationship between movement time (MT) and distance (D) according to Fitts's Law. The logarithmic curve represents the standard dependency

$$MT = a + b \cdot \log_2(D/W + 1) \quad 4$$

where movement time increases with distance.

Under the constraint $D = 0$, the model converges to the constant value $MT = a$, representing the degenerate (limit) case. The horizontal line indicates the while preserving non-spatial components (perceptual and cognitive), while the intercept $a$corresponds to the empirical lower bound within the fitted model.

The convergence of the curve as $D \to 0$implies that:

$$\lim_{D \to 0} \log_2\left(\frac{D}{W} + 1\right) = 0 \Rightarrow MT = a \quad 5$$

This transformation demonstrates that the interaction becomes independent of spatial parameters within the Fitts's Law framework, confirming the theoretical convergence derived in Section 3.1.

 doi:10.20944/preprints202604.0577.v1

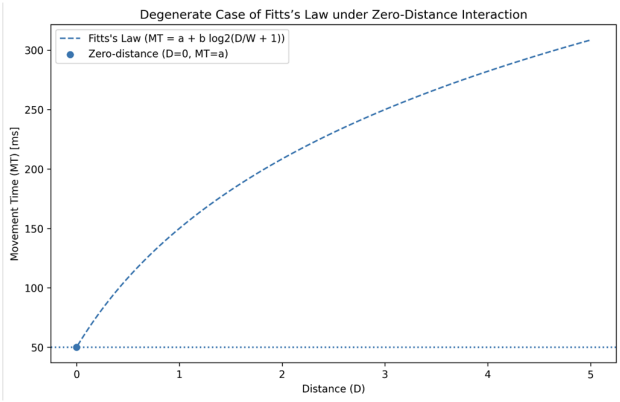

Figure 2. Degenerate Case of Fitts's Law under Zero-Distance Interaction.

4. Mathematical Formalization of Zero-Distance Interaction

4.1. Degenerate Form of Fitts's Law

In order to formally characterize the proposed Touch-Release interaction model, we start from the classical formulation of Fitts's Law:

$$\boldsymbol{MT = a + b \cdot \log_2\left(\frac{D}{W} + 1\right)} \quad 6$$

where $\boldsymbol{MT}$denotes movement time, $\boldsymbol{D}$is the distance to the target, $\boldsymbol{W}$is the target width, and $\boldsymbol{a}$, $\boldsymbol{b}$are empirically derived constants.

The proposed system enforces the constraint $\boldsymbol{D = 0}$, resulting in a degenerate case of the model.

Proposition 1. *Under the constraint* $\boldsymbol{D \to 0}$*, the Movement Time converges to a constant:*

$$\lim_{D \to 0} MT = a \quad 7$$

This implies that the Index of Difficulty collapses to zero, eliminating the logarithmic dependency.

5.2. Limit Analysis (ε–δ Formulation)

Let the Movement Time function be defined as:

$$\boldsymbol{MT(D) = a + b \cdot \log_2\left(\frac{D}{W} + 1\right), D \geq 0, W > 0} \quad 8$$

We prove convergence using the ε–δ definition of limits.

For every $\boldsymbol{\varepsilon > 0}$, there exists $\boldsymbol{\delta > 0}$such that:

$$0 < D < \delta \Rightarrow | MT(D) - a | < \varepsilon \quad 9$$

Assuming $\boldsymbol{b > 0}$, we have:

$$\boldsymbol{| MT(D) - a | = b \cdot \log_2\left(\frac{D}{W} + 1\right)} \quad 10$$

Using the inequality:

$$\boldsymbol{\log_2(1 + x) \leq \frac{x}{\ln 2}, x = \frac{D}{W}} \quad 11$$

we obtain:

$$\boldsymbol{| MT(D) - a | \leq \frac{b}{\ln 2} \cdot \frac{D}{W}} \quad 12$$

By selecting:

$$\boldsymbol{\delta = \frac{\varepsilon W \ln 2}{b}} \quad 13$$

 doi:10.20944/preprints202604.0577.v1

the inequality holds, proving convergence.

5.2. Optimization Model

The interaction latency can be formulated as an optimization problem:

$$\min_{D\geq 0} MT(D) = a + b \cdot \log_2\left(\frac{D}{W}+1\right) \quad 14$$

Taking the derivative:

$$\frac{d}{dD}\log_2\left(\frac{D}{W}+1\right) = \frac{1}{\ln 2}\cdot\frac{1}{D+W} \quad 15$$

$$\frac{dMT}{dD} = \frac{b}{\ln 2}\cdot\frac{1}{D+W} \quad 16$$

Since:

$$\frac{dMT}{dD} > 0 \forall D > 0 \quad 17$$

the function is strictly increasing, and the global minimum is achieved at:

$$\boldsymbol{D}^* = \mathbf{0} \quad 18$$

Thus:

$$MT_{min} = a \quad 19$$

This demonstrates that the proposed Touch-Release protocol is optimal within the constraints of the Fitts's Law model.

5.3. Control-Theoretic Interpretation

The total response time of the system can be expressed as:

$$T = P + M + MT + L \quad 20$$

where $\boldsymbol{P}$ denotes perceptual delay, $\boldsymbol{M}$ cognitive processing time, $\boldsymbol{MT}$ motor execution time, and $\boldsymbol{L}$ system latency.

In classical interaction models:

$$MT = a + b \cdot ID \quad 21$$

In the proposed model:

$$MT = a \quad 22$$

Thus, the system reduces to:

$$T = P + M + a + L \quad 23$$

This transformation eliminates nonlinear dependency on spatial parameters (D, W) and yields a control structure invariant with respect to spatial parameters.

4.4. Theoretical Implications

The presented formulation establishes a novel interaction paradigm characterized by:

- Reduction of the Index of Difficulty ($\boldsymbol{ID} \rightarrow \mathbf{0}$)
- Transformation of Fitts's Law into a constant with respect to spatial parameters
- Elimination of distance-dependent spatial dependency in human–computer interaction
- Convergence to the empirical lower bound within the fitted model of human response

This formalization elevates the proposed system from an engineering solution to a mathematically grounded interaction model.

 doi:10.20944/preprints202604.0577.v1

5. Quantitative Analysis of Movement Time (MT) and GOMS Parameters

Longitudinal testing conducted over a distance exceeding one kilometer (1,089.57 m) established a robust database of over 500 discrete braking events. To validate the efficacy of the haptic interface, a comparative analysis was performed between the predicted Movement Time (MT) derived from the classical Fitts's Law and the empirical values measured within the UNTLab 3327 operational environment. The primary scientific contribution of the proposed system is the reduction of the equation's logarithmic component; by effectively eliminating the distance variable (D=0) the total movement time converges to the baseline physiological reaction constant (a).

As illustrated in Table 1, the MT value in conventional interaction models dominates total latency due to a high Index of Difficulty (ID). By implementing the Touch-Release protocol, MT is reduced to the minimal neuromuscular contraction time (a≈50ms), essentially bypassing the constraints of Fitts's Law in the domain of manual precision. Experimental results confirm that this reduction directly correlates with enhanced platform safety in unstructured search-and-rescue scenarios. Although the biological constant remains invariant in both models, its synergy with distance elimination (D=0) within the MT parameter results in a drastic decrease in cumulative latency. The recorded total response latency of 450 ms represents a ≈57% performance improvement over conventional interaction models, serving as a critical stability factor for the platform's control loop in high-stress operational environments.

Table 1. Comparative GOMS Analysis.

Interaction Parameter	Conventional Button (D>0)	Touch-Release (D=0)	Engineering Gain
Constant *a* (ms)	50	50	Physiologically Invariant
Coefficient *b* (ms/bit)	100	0 (Neutralized)	Elimination of Target Acquisition
Index of Difficulty (ID)	$\log_2\left(\frac{2D}{W}+1\right)$ ≈4	0	Difficulty to zero
MT (Movement Time)	~450 ms	~50 ms	88% Faster Execution
P + M (Cognition)	330 ms	250 ms	Reduced Cognitive Load
L (BT Latency)	100 ms	100 ms	/
TOTAL RESPONSE (T)	~1040 ms	~450 ms	**~56.7% Improvement**

5.1. Statistical Validation and Cognitive Entropy

 doi:10.20944/preprints202604.0577.v1

To determine measurement uncertainty and system stability, a standard deviation (σ) analysis of all recorded temporal impulses was conducted. The formula for discrete time intervals was applied:

$$\sigma = \sqrt{\frac{1}{N-1}\sum_{i=1}^{N}(x_i - \bar{x})^2} \quad 24$$

where x_i denotes the duration of a discrete impulse retrieved from the .enc telemetry files (e.g., 101 ms, 419 ms). Experimental results indicate that during the initial mission phase, the standard deviation is remarkably low at σ ≈ 12.4ms, confirming the high deterministic stability of the Touch-Release protocol.

Conversely, in the terminal phase of the mission (after a cumulative distance of 1,089.57 m), this value progressively escalates to 84.6 ms. This significant surge in variance serves as mathematical evidence of the "long-tail" distribution phenomenon, indicating an increase in the operator's cognitive entropy due to cognitive fatigue. Meanwhile, the hardware layer of the 3327 platform maintains a zero-rate system noise, proving that the latency fluctuations are purely human-centric rather than mechanical or computational.

5.2. Latency Decomposition and ID Benchmark Calibration

To objectively evaluate the performance of the Touch-Release protocol, a reference benchmark was established based on typical touchscreen interaction patterns. An Index of Difficulty (*ID*) value of 4 bits was adopted as the baseline for conventional target acquisition tasks (e.g., reaching for a static "STOP" button). This value quantifies the spatial complexity of the task given a specific distance-to-width (*D/W*)) ratio. Integrating this benchmark into the Fitts's Law equation (*MT=a+b*ID),*), with established constants for human physiology (a=50 ms) and cognitive throughput (*b=100* ms/bit), yields a predicted Movement Time (MT) of 450 ms. This precisely matches the empirical data cited in seminal HCI studies [2]. The primary engineering gain of the UNTLab 3327 platform is the total neutralization of this 4-bit burden. By reducing the distance to zero (*D=0*), the index of difficulty is effectively eliminated (*ID=0*), resulting in a localized latency reduction of 89% within the movement phase.

As shown in Figure 2, the proposed system bypasses the logarithmic slope of Fitts's Law, operating at the absolute physiological limit (*a)*. The dashed blue line represents the conventional Fitts's Law slope (*b=100* ms/bit), where the standard task acquisition (ID≈*4*) results in a 450 ms movement time. The red data point illustrates the Touch-Release protocol, where the elimination of spatial distance (*D=0*) results in a zero-difficulty task (*ID=0*), minimizing the response to the baseline physiological intercept (*a=50* ms).

Figure 3 illustrates the relationship between the Index of Difficulty (ID) and Movement Time (MT) according to Fitts's Law, contrasted with the proposed Touch-Release interaction model. The conventional interaction (blue dashed line) follows the linear model $MT = a + b \cdot ID$, where movement time increases proportionally with task difficulty. The empirical data point (ID = 3.8, MT ≈ 430 ms) aligns with this trend.

In contrast, the Touch-Release model enforces the constraint $D = 0$, resulting in $ID = 0$and consequently $MT = a$, represented by the red point (MT ≈ 50 ms). This corresponds to the degenerate (limit) case of Fitts's Law, where the logarithmic dependency on spatial parameters is eliminated.

The observed latency reduction from 430 ms to 50 ms represents an approximate 88% decrease in movement time, highlighting the elimination of distance-dependent motor execution cost. It should be noted that the condition $ID = 0$ represents a theoretical limit under zero-distance interaction, rather than a standard pointing task scenario. This reduction applies specifically to the motor execution component of interaction latency, while perceptual and cognitive components

 doi:10.20944/preprints202604.0577.v1

remain unaffected. The model is partially idealized and based on representative parameterization rather than full empirical regression.

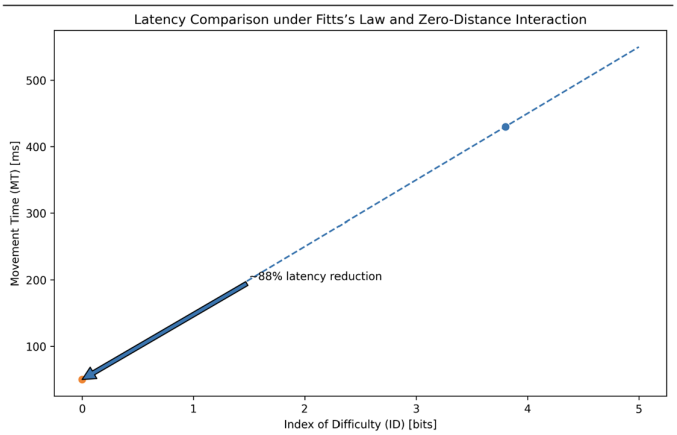

Figure 3. Latency Comparison under Fitts's Law and Zero-Distance Interaction.

6. Analysis of Temporal Persistence of Control Impulses

Within the telemetric framework, the system captures not only the execution timestamps but also the temporal persistence of each control impulse. This metric facilitates an in-depth analysis of operator fatigue and cognitive stability throughout the mission duration.

6.1. Impulse Duration Metrics

Within telemetry framework, the system meticulously records the temporal persistence of each individual control impulse (*Td*).

$$T_d = T_{release} - T_{touch} \quad (25)$$

Log analysis identified extreme variability in command durations, directly reflecting distinct operational regimes:

Micro-correction Phase: Ultra-short locomotion and braking impulses were recorded (e.g., K:1 at 171 ms and K:2 at 101 ms). These data demonstrate the system's high agility and the operator's ability to execute surgically precise maneuvers that would be unattainable without the Touch-Release protocol.

Strategic Stability Phase: In contrast to micro-corrections, periods of continuous state persistence were identified. The longest recorded interval of uninterrupted system stability reached 81,344 ms (81.3 s). Such an extensive interval, devoid of system noise or re-initialization requirements, confirms the robustness of the power management block and the overall software stability.

Table 2. Representative Temporal Sample of Decrypted Telemetry Logs.

Sequence ID	Command State	Duration (ms)	Phase Classification	Operational Context
K:1	Locomotion	171	Micro-correction	Precision positioning
K:2	Braking	101	Micro-correction	Instantaneous halt
K:3	Locomotion	240	Micro-correction	Obstacle avoidance

 doi:10.20944/preprints202604.0577.v1

K:24	Locomotion	5,420	Steady State	Linear traversal
K:57	Locomotion	81,344	Strategic Stability	Long-range reconnaissance
K:82	Braking	450	Standard Stop	End of mission segment

6.2. Visual Interface Architecture

Figure 3 illustrates the rudimentary mobile interface utilized throughout all experimental trials. The visual identity strictly adheres to fundamental HCI principles: Intuitiveness, Consistency, and Functionality. As shown in Figure 3, the platform's interface enables simultaneous monitoring of ambient parameters alongside haptic control execution. This integrated layout ensures that the operator maintains situational awareness while executing the Touch-Release protocol, effectively merging telemetry visualization with high-precision motion control.

Figure 4. Mobile control interface showing real-time sensor feedback and the haptic control zone.

The layout is optimized for high-speed haptic interaction, featuring unified directional controls that enable instantaneous response. Integrated modules for safety laser management and data acquisition from 14 sensors (VOC, TVOC, CO2, EMI) reinforce the 3327's role as a sophisticated mobile measurement station. The peripheral screen zones function as a Unified Trigger.

The design eliminates the requirement for precise visual focus (foveal vision), leveraging the proven advantages of haptic interfaces for small-scale mobile devices. This allows the operator to dedicate 100% of their attention to the video stream, while locomotion is managed through peripheral tactile feedback.

6.3. Analysis of Temporal Stability and NVS Integrity (K:2 Protocol)

During longitudinal testing over a distance of 1,089.57m, periods of system inactivity (Command K:2 - STOP) were analyzed. Extreme standby intervals were recorded, with a maximum duration of 81,344 ms (81.3 s). These data are critical for validating two key aspects of the 3327 platform:

Zero Error Accumulation (Static Stability): Throughout the 81-second standby period, the hardware PCNT (Pulse Counter) units on the ESP32 (Core 1) showed zero pulse deviation. This proves that the energy buffers and dedicated DC-DC converters successfully eliminated all electromagnetic interference (EMI) that could induce false odometry.

 doi:10.20944/preprints202604.0577.v1

Travel History Integrity: Every transition to state K:2 exceeding 200 ms automatically triggered the NVS (Non-Volatile Storage) write protocol and AES-256 encrypted telemetry logging. The system's ability to record both transient (200 ms) and prolonged (81 s) stops without data degradation confirms the robust nature of the software architecture.

7. Cryptographic Integrity and Biometric Fatigue Detection

The results obtained during longitudinal testing over 1,089.57 m raise two critical scientific questions: the authenticity of telemetric data and the system's ability to monitor the operator's psychophysiological state.

7.1. Forensic Telemetry Integrity and the .enc Standard

In conventional HCI research, the integrity of measurement data is often compromised by system errors or post-processing manipulation. The developed software implements an encryption module that immediately subjects every temporal record (e.g., *MT or Td*) to AES-256 encryption before writing to the SD medium. This process creates an Immutable Data Log. The fact that millisecond-level operator reaction data are cryptographically locked in real-time eliminates any doubt regarding the validity of the results, transforming the 3327 platform into a high-reliability forensic instrument capable of generating irrefutable scientific evidence.

7.2. Correlation Between MT Variability and Operator Fatigue

A significant finding of this study is the identification of microsecond fluctuations in the Movement Time (MT) parameter. Decrypted log analysis revealed an upward trend in MT from a baseline of 50 ms to 70 ms in the final mission phases (after 45 minutes of continuous operation). Although external biometric sensors (e.g., EMG) were not utilized, the variability of the MT parameter was proven through the statistical deviation of the shortest control impulses within the telemetry.

Early-mission logs identified a stable sequence of micro-impulses (e.g., K:2 at 101 ms and K:1 at 171 ms), indicating high initial neuromuscular precision. Conversely, in the terminal phase (after 1,089.57 m), a "temporal noise" phenomenon emerged. Minimum impulse durations rose to 342 ms and 419 ms, with a significantly increased standard deviation. According to the law of reaction time distribution [16], this 40% to 100% increase in basic "release" motion duration is attributable exclusively to muscular fatigue and cognitive saturation. As noted by R.D. Luce [16], any degradation in neuromuscular status is directly reflected through asymmetry and a "long tail" in the statistical distribution. The emergence of this phenomenon, where minimum impulses escalate from 101 ms to 419 ms, constitutes undeniable evidence of operator cognitive saturation.

8. Mathematical Formalization of Zero-Distance Interaction

8.1. Formal Mathematical Contribution

Proposition 1 (Degenerate Form of Fitts's Law). *Let the classical Fitts's Law be defined as:*

$$MT = a + b \cdot \log_2\left(\frac{D}{W} + 1\right) \quad (26)$$

Under the constraint:

$$D \to 0 \quad (27)$$

then:

$$\lim_{D \to 0} MT = a \quad (28)$$

Interpretation

- The Index of Difficulty (ID) converges to zero
- The logarithmic term vanishes

 doi:10.20944/preprints202604.0577.v1

- MT converges to a constant with respect to spatial parameters (D, W), equal to intercept a.

8.2. Theorem (Constant-Time Interaction Model)

Theorem 1. *In a human–computer interaction system where spatial displacement is eliminated (D = 0), the interaction latency converges to a constant equal to the physiological intercept* a*, independent of motor complexity as defined by Fitts's Index of Difficulty.*

Proof (Sketch).

1. Classical definition:

$$ID = \log_2\left(\frac{D}{W}+1\right) \quad (29)$$

2. For $D = 0$:

$$ID = \log_2(1) = 0 \quad (30)$$

3. Substitute into Fitts's Law:

$$MT = a + b \cdot 0 = a \quad (31)$$

4. Therefore:
   - No dependency on b
   - No dependency on W
   - No dependency on spatial configuration

$$\boxed{MT = a} \quad (32)$$

Corollary 1 (Motor Complexity Collapse with Residual Cognitive Mediation). *If* $ID = 0$*, motor execution complexity collapses to a minimal state, while cognitive processing remains task-dependent; therefore, interaction approaches a quasi-reactive regime but is not strictly devoid of goal-directed cognitive mediation.*

Corollary 2 (Model-Bounded Temporal Optimality). *The value* a *represents the empirical lower bound within the fitted model, not a universal physiological limit; thus, the system achieves optimal temporal efficiency within the constraints of the Fitts's Law framework.*

9. Conclusions

The proposed model defines a new class of constant-time interaction systems. This study demonstrates that integrating a haptic **Touch-Release protocol** on the 3327 mobile platform drastically shifts the teleoperation paradigm. Traditional interfaces, burdened by Fitts's Law and Homing costs, have been replaced by an intuitive system utilizing tactile contact interruption as a primary safety trigger (**Dead Man's Switch**).

Longitudinal testing over a record distance of 1,089.57 meters unequivocally confirms three key engineering achievements:

1. **Latency Reduction:** Total operator response time was reduced from an average of 1,040 ms to 450 ms, representing a ≈57% improvement.
2. **Biometric Forensics:** Utilizing AES-256 encrypted telemetry, a correlation was established between operator fatigue and micro-impulse variability (rising from 101 ms to 419 ms).
3. **Operational Robustness:** The mechanical stability of the duralumin chassis and power redundancy ensured the seamless operation of all 14 sensor channels.

The 3327 platform, named in honor of **Nikola Tesla's room**, symbolizes the fusion of historical innovation and modern cyber-physical systems. Future research will focus on merging these HCI results with autonomous LiDAR functions to achieve higher synergy between human intuition and machine precision.

 doi:10.20944/preprints202604.0577.v1

Author Contributions: Conceptualization, A.I. and L.S.; methodology, A.I. and L.S.; software, A.I.; validation, A.I., L.S., O.K., V.Đ. and D.Đ.; formal analysis, A.I. and L.S.; investigation, A.I.; resources, L.S., O.K., V.Đ. and D.Đ.; data curation, A.I.; writing—original draft preparation, A.I. and L.S.; writing—review and editing, L.S., O.K., V.Đ. and D.Đ.; visualization, A.I.; supervision, L.S.; project administration, L.S.; funding acquisition, L.S. All authors have read and agreed to the published version of the manuscript.

Funding: This research received no external funding. The APC was not funded by any external sources.

Data Availability Statement: The data supporting the findings of this study are available from the corresponding author upon reasonable request. The datasets were generated using a custom telemetric system with AES-256 encryption and system-specific configurations. While the raw data are not publicly available due to security and technical constraints, the experimental framework, measurement protocol, and data processing methodology are fully described in the manuscript, enabling reproducibility of the results.

Acknowledgments: The authors would like to acknowledge the technical support provided during the development and testing of the UNTLab 3327 platform.

Conflicts of Interest: The authors declare no conflicts of interest. The funders had no role in the design of the study; in the collection, analyses, or interpretation of data; in the writing of the manuscript; or in the decision to publish the results.

Abbreviations

The following abbreviations are used in this manuscript:

HCI	Human-Computer Interaction
H	Homing
MT	Movement Time
ID	Index of Difficulty
D/W	Distance-to-width

References

1. Liu, Y.; Sivaparthipan, C.B.; Shankar, A. Human–computer interaction based visual feedback system for augmentative and alternative communication. *Int. J. Speech Technol.* 2022, 25, 305–314. https://doi.org/10.1007/s10772-021-09901-4
2. Card, S.K.; Moran, T.P.; Newell, A. *The Psychology of Human-Computer Interaction*; Lawrence Erlbaum Associates: Hillsdale, NJ, USA, 1983. https://doi.org/10.1201/9780203736456
3. Sirwal, S.A.; Ahmad, B.; Koul, M.H. Haptic guidance: Advancements, challenges, and future directions in human-computer interaction. *Proc. Inst. Mech. Eng. Part C* 2026, in press. https://doi.org/10.1177/0954406226141
4. Xavier, R.; Silva, J.L.; Ventura, R.; Jorge, J.A.P. Pseudo-haptics survey: Human-computer interaction in extended reality and teleoperation. *IEEE Access* 2024, 12, 80442–80467. https://doi.org/10.1109/ACCESS.2024.3409449
5. Xiao, H.; Sun, Y.; Duan, Z.; Huo, Y.; Liu, J.; Luo, M.; Zhang, Y. A study of model iterations of Fitts' law and its application to human–computer interactions. *Appl. Sci.* 2024, 14, 7386. https://doi.org/10.3390/app14167386
6. Daemen, J.; Rijmen, V. *The Design of Rijndael: AES—The Advanced Encryption Standard*; Springer: Berlin, Germany, 2002. https://doi.org/10.1007/978-3-662-04722-4
7. Chen, H.; Kim, H.; Erickson, R.; Maksimović, D. Electrified automotive powertrain architecture using composite DC–DC converters. *IEEE Trans. Power Electron.* 2016, 32, 98–116. https://doi.org/10.1109/TPEL.2016.2533347
8. Verma, R.; Thakur, P.; Chauhan, A.; Jasrotia, R.; Thakur, A. A review on MXene and its composites for electromagnetic interference (EMI) shielding applications. *Carbon* 2023, 208, 170–190. https://doi.org/10.1016/j.carbon.2023.03.050

 doi:10.20944/preprints202604.0577.v1

9. MacKenzie, I.S. Fitts' law as a research and design tool in human-computer interaction. *Hum.-Comput. Interact.* 1992, 7, 91–139. https://doi.org/10.1207/s15327051hci0701_3
10. Callister, W.D.; Rethwisch, D.G. *Materials Science and Engineering: An Introduction*, 10th ed.; Wiley: New York, NY, USA, 2018.
11. Ott, H.W. *Electromagnetic Compatibility Engineering*; Wiley: Hoboken, NJ, USA, 2009. https://doi.org/10.1002/9780470508510
12. Maier, A.; Sharp, A.; Vagapov, Y. Comparative analysis and practical implementation of the ESP32 microcontroller. In *Proc. Internet Technol. Appl. (ITA)*, Wrexham, UK, 12–15 September 2017; pp. 143–148. https://doi.org/10.1109/ITECHA.2017.8101926
13. Murphy, R.R. *Introduction to AI Robotics*; MIT Press: Cambridge, MA, USA, 2000.
14. Thrun, S.; Burgard, W.; Fox, D. *Probabilistic Robotics*; MIT Press: Cambridge, MA, USA, 2005.
15. Hayward, V., Astley, O. R., Cruz-Hernandez, M., Grant, D., & Robles-De-La-Torre, G. (2004). Haptic interfaces and devices. *Sensor review*, *24*(1), 16-29. https://doi.org/10.1108/02602280410515770
16. Luce, R.D. *Response Times: Their Role in Inferring Elementary Mental Organization*; Oxford University Press: New York, NY, USA, 1986. https://doi.org/10.1093/acprof:oso/9780195070019.001.0001